scanner (75% correct on average) did not differ during blank, sequential, or simultaneous presentation periods [$F(2, 143) = 1.60$, $P = 0.21$]. Hence, neither presentation condition interfered with the T/L task, indicating that this task provided sufficient attentional load to preclude exogenous attentional cueing.

7. The borders of retinotopic areas in the ventral extrastriate cortex of humans and monkeys [R. Gattass, C. G. Gross, J. H. Sandell, *J. Comp. Neurol.* **21**, 519 (1981); R. Gattass, A. P. Sousa, C. G. Gross, *J. Neurosci.* **8**, 1831 (1988); M. I. Sereno *et al.*, *Science* **268**, 889 (1995); R. B. H. Tootell *et al.*, *J. Neurosci.* **15**, 3215 (1995); E. A. DeYoe *et al.*, *Proc. Natl. Acad. Sci. U.S.A.* **93**, 2382 (1996)] are formed by the representations of either the vertical (V1/V2 or VP/V4) or the horizontal (V2/VP) meridians. Meridians were mapped with color- and luminance-contrast checkered stimuli. In five of eight participants, it was difficult to determine the extent of VP, because the representations of the V2/VP and the VP/V4 border were abutting or overlapping [see S. Shipp, J. D. G. Watson, R. S. J. Frackowiak, S. Zeki, *Neuroimage* **2**, 125 (1995)]. We will, therefore, refer to the area between the V1/V2 border and the VP/V4 border as "V2", although it likely contains parts of VP. The presumptive lower field representation of V4 was determined with the complex images presented to the lower field and was found to be located adjacent and lateral to V4's upper field representation on the fusiform gyrus [D. J. McKeefry and S. Zeki, *Brain* **120**, 2229 (1997)]. The region we have termed V4 may include all or part of the region termed V8 by Hadjikhani *et al.* [*Nature Neurosci.* **1**, 235 (1998)]. In the region located anterior to V4 (and also V8), the spatial segregation of upper and lower field representations was no longer seen, suggesting that this area was different from V4. Because area TEO is located just anterior to V4 in the monkey [D. Boussaoud, R. Desimone, L. G. Ungerleider, *J. Comp. Neurol.* **306**, 554 (1991)], we will refer to this similarly located area as putative human TEO.
8. In a separate experiment, four stimuli (each 0.5° × 0.5° in size) were presented 6° apart from each other in the right upper quadrant. The prediction was that increasing the spatial separation between stimuli would strongly reduce suppressive interactions in areas with small (V2) and intermediate (V4) receptive fields but not in areas with large receptive fields (TEO) extending over a quadrant. Results from three participants showed that the interactions were indeed abolished in V2, were strongly reduced in V4, but were still present in TEO.
9. Three of the eight participants saw complex stimuli at 1 Hz in the following presentation configurations: one stimulus presented to the upper visual field, three presented to the lower visual field, or all four presented together. Participants performed the T/L task at fixation throughout the scan. All other presentation parameters were as in experiment 1.
10. The averaged signal changes in V4's upper field were 1.04% evoked by the single stimulus, 0.83% evoked by the four stimuli, and 0.52% evoked by the three stimuli in the lower field (due to signal spread into the upper field). Because of this spread, the actual suppression effect might be much larger than that reflected in the difference in responses to the single stimulus and to the four stimuli. The response differences were not significant in V1 and V2. Thus, with this experimental design, suppressive interactions could only be demonstrated in areas with sufficiently large receptive fields.
11. All four stimuli, including the stimulus selected to be the target, were randomly presented in all four locations in blocks of 15 s. The blocks with directed attention to the stimulus display were indicated by a marker presented close to the fixation point 1 s before the block started. In pilot experiments, we found that the attentional effect during the first attended block in a sequence was always stronger than in other attentional blocks within a run. To attenuate this attentional "onset" effect, each run started with a block of attended presentations that was discarded from analysis.
12. Before being scanned, participants received training in the directed attention task and fixation was monitored. During the directed attention task, targets were identified correctly at rates of 86 and 93%, respectively, in the sequential and simultaneous presentation conditions. The attentional load of the T/L task and the directed attention task was assessed by having participants perform them simultaneously in tests conducted outside the scanner. Both tasks interfered with each other when performed simultaneously. Performance in the directed attention task dropped significantly [$F(1, 192) = 130.92$, $P < 0.0001$] from 86 to 45% and from 93 to 49%, respectively, in the sequential and simultaneous conditions. Likewise, performance in the T/L task dropped significantly [$F(1, 191) = 66.76$, $P < 0.0001$] when participants were required to simultaneously identify targets at the target location. Thus, both tasks had a high attentional load. Participants rarely identified target stimuli in locations other than the attended location.
13. Because the cortical activations from the attended and unattended stimuli could not be separated, any increase in response to the attended stimulus might, in principle, be counterbalanced by a decrease in response to an unattended one, working against our hypothesis. However, the attended stimulus was located closest to the fovea and thus would dominate the response to the array because of the cortical magnification factor. Further, single-cell studies have shown that attention to a stimulus filters out the suppressive influence of nearby stimuli very effectively, but it has a smaller suppressive effect on the response to unattended ones (R. Desimone, unpublished observations).
14. Cortical volumes activated in the unattended condition were 394 mm^3 in V1, 400 mm^3 in V2, 1600 mm^3 in V4, and 1156 mm^3 in TEO, averaged over participants. In the attended condition, brain volumes increased significantly in V4 and TEO but not in V1 and V2 [V4: 78 ± 16% (mean ± SEM); TEO: 120 ± 36%; ANOVA, main attentional effect: $F(1, 64) = 14.2$, $P < 0.001$; cortical area and attentional effect: $F(3, 64) = 2.82$, $P < 0.05$].
15. H. J. Heinze *et al.*, *Nature* **372**, 543 (1994); G. R. Mangun, *Psychophysiology* **32**, 4 (1995); G. Rees, R. Frackowiak, C. Frith, *Science* **275**, 835 (1997); R. Vandenberghe *et al.*, *J. Neurosci.* **17**, 3739 (1997).

16. We thank J. M. Maisog, M. I. Elizondo, and M. A. Georgopoulos for help with data analysis; P. Jezzard for help with scanning; and J. V. Haxby, B. Jagadeesh, A. Martin, J. Reynolds, and U. Ziemann for valuable discussions. S.K. was supported by the Deutsche Forschungsgemeinschaft.

11 May 1998; accepted 4 August 1998

A Structural Basis for Recognition of A·T and T·A Base Pairs in the Minor Groove of B-DNA

Clara L. Kielkopf, Sarah White, Jason W. Szewczyk, James M. Turner, Eldon E. Baird, Peter B. Dervan,* Douglas C. Rees*

Polyamide dimers containing three types of aromatic rings—pyrrole, imidazole, and hydroxypyrrole—afford a small-molecule recognition code that discriminates among all four Watson-Crick base pairs in the minor groove. The crystal structure of a specific polyamide dimer-DNA complex establishes the structural basis for distinguishing T·A from A·T base pairs. Specificity for the T·A base pair is achieved by means of distinct hydrogen bonds between pairs of substituted pyrroles on the ligand and the O2 of thymine and N3 of adenine. In addition, shape-selective recognition of an asymmetric cleft between the thymine-O2 and the adenine-C2 was observed. Although hitherto similarities among the base pairs in the minor groove have been emphasized, the structure illustrates differences that allow specific minor groove recognition.

Before the first structure of a molecule bound to DNA had been determined, specific recognition of double helical B-form DNA was predicted to occur primarily in the major, rather than the minor, groove (*1*). This proposal was based on the observation that for A,T base pairs, the hydrogen bond acceptors at N3 of adenine and O2 of thymine are similarly placed and lack any prominent distinguishing feature (*1*) (Fig. 1). Subsequent structures of DNA binding domains cocrystallized with DNA supported this idea, because most of the specific contacts were made with the major groove (*2*). The principle that "the major groove is a better candidate for sequence-specific recognition than the minor groove" (*3*) continues to provide the basis for strategies to decipher rules for

C. L. Kielkopf, Division of Biology, California Institute of Technology, Pasadena, CA 91125, USA. S. White, J. W. Szewczyk, J. M. Turner, E. E. Baird, P. B. Dervan, Division of Chemistry and Chemical Engineering, California Institute of Technology, Pasadena, CA 91125, USA. D. C. Rees, Howard Hughes Medical Institute and Division of Chemistry and Chemical Engineering, California Institute of Technology, Pasadena, CA 91125, USA.

*To whom correspondence should be addressed. E-mail: dervan@its.caltech.edu (P.B.D.); dcrees@its.caltech.edu (D.C.R.)

protein-DNA recognition.

Although there has been remarkable progress in the design of zinc fingers to recognize the major groove (*4*), no protein structure motif has been identified that provides an α-amino acid–base pair code for the minor groove. Eight-ring hairpin polyamides have affinities and specificities that rival those of major groove–binding proteins (*5*) and have been shown to permeate living cells and inhibit specific gene expression (*6*). The side-by-side pairing of the residues in the polyamide dimer determines the DNA sequence recognized. An imidazole (Im)/pyrrole (Py) pair distinguishes G·C from C·G and both of these from A·T and T·A base pairs (*5*), and the structural basis of this discrimination is now understood (*7*). However, a structural understanding for how a hydroxypyrrole (Hp)/Py pair distinguishes T·A from A·T and both of these from G·C and C·G (*8*) has yet to be established. To address this question, we determined the cocrystal structure of a polyamide of sequence ImHpPyPy-β-Dp (Fig. 2A), bound as a dimer to a self-complementary 10–base pair oligonucleotide containing all four Watson-Crick base pairs, 5′-CC**AGTACT**GG-3′ (binding site in bold; β, β-alanine; Dp, dimethylamino-propylamide) (Fig. 2B and Table 1). The structure of the polyamide ImPyPyPy-β-Dp, containing a Py-Py pair that does not distinguish A·T and T·A (*9, 10*), bound to the same duplex was solved for comparison. In both the ImHpPyPy and ImPyPyPy structures, the polyamides bind as antiparallel dimers centered over the target GTAC sequence in the minor groove of a B-form DNA duplex (Fig. 2B). The NH_2- to COOH-terminal orientation of each fully overlapped polyamide is parallel to the adjacent 5′-to-3′ strand of DNA, consistent with previous chemical (*11*) and structural studies of polyamide dimers (*7, 10, 12, 13*).

Although the functional groups of adenine and thymine are very similar in the minor

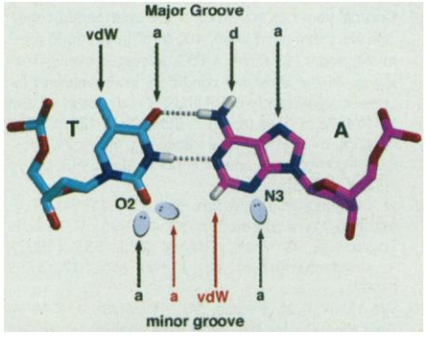

Fig. 1. Anatomy of the T·A base pair. Arrows indicate potential sites for discrimination of A·T from T·A in the major and minor grooves. Lone pair electrons in the minor groove are shown as ovals, and Watson-Crick hydrogen bonds of the base pair as dotted lines. Arrows for previously described sites (*1*) are black, and sites identified in this report are red. The type of potential recognition is labeled: a, hydrogen bond acceptor; d, hydrogen bond donor; and vdW, van der Waals.

Table 1. Data collection and refinement statistics. The ImHpPyPy and ImPyPyPy structures crystallized in an isomorphous lattice (*22*) and were solved by molecular replacement with a B-DNA model (*23*). The ImHpPyPy data were collected on beamline 9-1 at the Stanford Synchrotron Radiation Laboratory (SSRL), with a MAR Research image plate detector at wavelength 0.98 Å. The ImPyPyPy data were collected on an R-Axis IIC image plate with CuKα radiation produced by a Rigaku RU200 rotating anode generator with double-focusing mirrors and a Ni filter. Both sets of data were collected on flash-cooled crystals. The data were processed with DENZO/SCALEPACK (*24*). Free-*R* sets comprising 5% of the data were chosen to contain the same reflections in resolution shells that overlapped between the data sets. All data were used, with bulk solvent correction and anisotropic B-scale applied with the program X-PLOR (*25*) and no sigma cutoff. The polyamide β-Dp tails of both structures were modeled in alternate conformations. The planarity of the bases, aromatic rings, and peptide bonds were restrained throughout the refinement. Topology and parameter files for polyamides and Tris were generated with XPLO2D (*26*), and nucleic acid parameters were those of Parkinson *et al.* (*27*).

Item	ImHpPyPy	ImPyPyPy
	*Data collection**	
Space group	C2	C2
Unit cell (Å)	a = 60.4, b = 30.5, c = 42.8 β = 120.5°	a = 60.7, b = 30.2, c = 43.5 β = 123.6°
Resolution (Å)	2.2–17.0	2.1–16.0
Measured reflections	9893	12267
Unique reflections	3070	3417
Completeness (%)	91.5 (91.0)	91.6 (82.9)
$I/\sigma(I)$	28.8 (3.2)	31.8 (4.1)
R_{sym}† (%)	3.0 (25.7)	3.8 (17.9)
	Refinement	
R_{cryst}‡ (%)	21.0	21.9
R_{free}‡ (%)	23.7	24.2
Rms deviation of bond lengths (Å)	0.016	0.012
Rms deviation of bond angles (°)	2.17	1.29
Number of nonhydrogen atoms		
DNA	404	404
Polyamide	96	96
Tris	8	–
Water molecules	65	87

*Values in parentheses are for the highest resolution shell: 2.28 to 2.20 Å for ImHpPyPy, and 2.18 to 2.10 Å for the ImPyPyPy data sets. †$R_{merge} = \Sigma_{hkl}\Sigma_i|I_i - \langle I\rangle|/\Sigma_{hkl}\Sigma_i\langle I\rangle$ where I_i is an intensity I for the ith measurement of a reflection with indices hkl and $\langle I\rangle$ is the weighted mean of all measurements of I. ‡$R_{cryst} = \Sigma_{hkl}||F_o(hkl)| - k|F_c(hkl)||/\Sigma_{hkl}|F_o(hkl)|$ for the working set of reflections, where F_o and F_c are the observed and calculated structure factors, respectively, and R_{free} is R_{cryst} for 5% of the reflections excluded from the refinement.

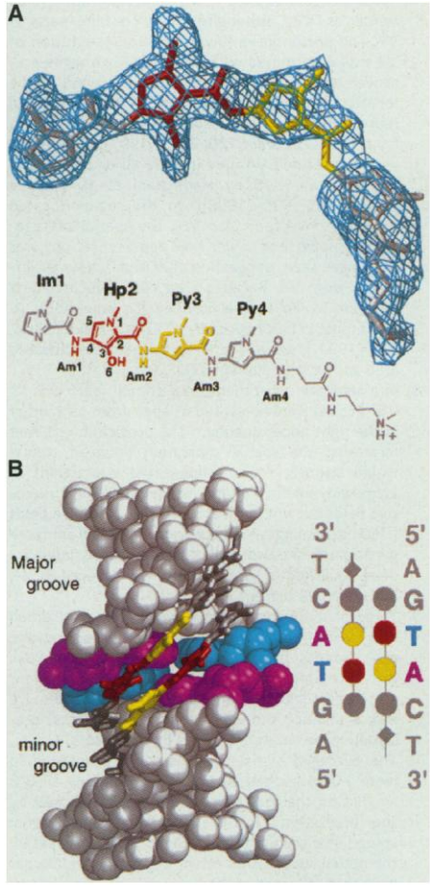

Fig. 2. (**A**) Omit $|F_o| - |F_c|$ electron density map for one of the ImHpPyPy polyamide molecules, contoured at 1.5σ, showing the position of the 3-hydroxyl group. The numbering of the atoms used in the text is indicated below on the chemical structure. The Hp is red and the Py that would be paired with it is yellow. The Im, the other Py, β, and Dp are silver. (**B**) Space-filling model of $(ImHpPyPy)_2$·5′-CC**AGTAC**-TGG-3′. Adenosine is purple and thymidine cyan; polyamide is colored as above. A schematic is shown to the right, with the aromatic residues of the polyamide indicated by filled circles and β by the diamonds. The overall structure of $(ImPyPyPy)_2$·5′-CC**AGTACT**GG-3′ is similar.

groove, the number of lone pairs on the hydrogen bond acceptors is different: a thymine-O2 has two free lone pairs, whereas an adenine-N3 has only one (Fig. 1). The amide nitrogens of the ligand form hydrogen bonds with the purine-N3 (A or G) or pyrimidine-O2 (T or C). As a result, the hydrogen bond potential of adenine-N3 is filled when a polyamide composed of imidazole or pyrrole residues is bound, but the thymine-O2 has the capacity to accept an additional hydrogen bond. We found that both the hydroxyl group of the Hp and the amide-NH of the preceding residue form hydrogen bonds with the target thymine-O2 of the adjacent DNA strand (Fig. 3A). A similar interaction between the Hp and the adenine-N3 would be impossible without loss of the hydrogen bond from the preceding amide-NH.

Although a hydrogen bond of favorable length (Table 2) is formed between Hp and thymine-O2, it was possible that the position of the hydroxyl and the amide out of the plane of the thymine-O2 sp^2-hybridized lone pairs would weaken the hydrogen bonds. The thymine-C2=Ô2···O6-Hp and thymine-C2=Ô2···N-amide angles and their out-of-plane and in-plane components were calculated to be 17° or 35° out of the plane, for the Hp and amide, respectively, and 25° in the plane (Table 2). The observed values for the components of the hydroxyl and amide hydrogen bond angles with thymine were found to be comparable to hydrogen bond angles between carbonyls and waters in protein structures, which range from ~0° to 60° for both the in- and out-of-plane angles (*14*). In addition, the out-of-plane thymine-C2=Ô2···N-amide components in the ImPyPyPy structure are approximately the same as those of ImHpPyPy, indicating that formation of an additional hydrogen bond with the hydroxyl does not substantially perturb the hydrogen bond geometry between the amide and the thymine-O2.

In addition to the difference in number of lone pairs of the adenine-N3 versus thymine-O2, adenine is also distinguished from thymine by a bulkier aromatic ring. Although the adenine-C2–H does not protrude into the minor groove like the guanine exocyclic amine, the additional carbon results in an asymmetric cleft in the minor groove of a T·A base pair (*8, 15*) (Fig. 1). The adenine-C2 of the ImHpPyPy structure contacts the Hp hydroxyl (Fig. 3B). Modeling the target thymine as an adenine reveals that the C2 carbon of a mismatch "adenine" opposite an Hp residue would sterically overlap the hydroxyl by 1 to 2 Å (depending on the hydrogen positions). Furthermore, the orientation of the Hp hydroxyl observed in the ImHpPyPy structure, 3.5 Å from the adenine-C2, with an average adenine-C2–H···O6-Hp angle of 165° (depending on the hydrogen positions) (Table 2), indicates that the Hp-O6 forms a favorable C–H hydrogen bond with the adenine-C2–H. As in this case, C–H hydrogen bonds are strongest between aromatic carbons adjacent to nitrogen atoms with oxygen hydrogen bond acceptors (*16*). Shape-selective recognition of the asymmetric cleft is the second feature that allows the Hp/Py pair to discriminate T·A from A·T.

The sugar-phosphate backbones in the ImHpPyPy and ImPyPyPy structures superimpose with 0.75 Å root-mean-square (rms) difference. In both structures, the oligonucleotides have the standard B-DNA features of 35° twist, 3.4 Å rise per residue, and C2′-endo sugar pucker, but they are distinguished

Table 2. Polyamide-DNA hydrogen bonds. Dashes indicate not applicable.

	*Hydrogen bond distance (Å) and donor-H···acceptor angle (°)**							
Polyamide-DNA atoms	ImHpPyPyβDp1 to DNA strand 1		ImHpPyPyβDp2 to DNA strand 2		ImPyPyPyβDp1 to DNA strand 1		ImPyPyPyβDp2 to DNA strand 2	
	Distance	Angle	Distance	Angle	Distance	Angle	Distance	Angle
Im1N3···GuaN2	3.0	157.5	3.0	152.8	3.2	163.5	3.2	157.3
Am1N···ThyO2	2.5	134.3	3.0	138.7	2.8	136.4	2.8	136.8
Am2N···AdeN3	3.2	144.0	3.8	148.1	3.0	156.2	2.8	159.0
Am3N···CytO2	3.5	147.1	3.4	135.0	3.1	157.2	2.9	166.3
Am4N···ThyO2	3.1	133.8	3.1	132.0	3.0	132.4	2.7	146.6
Hp2O6···AdeC2	3.5	160.0	3.4	179.0	–	–	–	–
Hp2O6···ThyO2	2.8	167.0	2.8	173.4	–	–	–	–
	ImHpPyPyβDp1, Intramolecular		ImHpPyPyβDp2, Intramolecular					
Hp2O6···Am2N	2.9	130.5	3.0	129.6	–	–	–	–

	Analysis of hydrogen bond acceptor angles (°) at the target thymines†			
Polyamide-DNA atoms	ImHpPyPyβDp1 to DNA strand 1	ImHpPyPyβDp2 to DNA strand 2	ImPyPyPyβDp1 to DNA strand 1	ImPyPyPyβDp2 to DNA strand 2
ThyC=Ô···HpO6	150 (145)	154 (155)	–	–
In-plane	21 (18)	28 (33)	–	–
Out-of-plane	16 (14)	18 (17)	–	–
ThyC=Ô···Am1N	142 (138)	144 (141)	147 (145.2)	132 (124.5)
In-plane	28 (21)	31 (21)	20 (6)	36 (33)
Out-of-plane	34 (43)	32 (40)	29 (36)	35 (48)

*Distances were measured between donor and acceptor atoms. Angles are those formed by donor-H···acceptor atoms. Hydrogens were assigned with standard geometry to sp^2-hybridized groups by use of X-PLOR (*25*). The hydroxyl hydrogen was assigned with standard bond length and angle in the orientation closest to the Thy-O2 yet having favorable staggered conformation with respect to the Hp ring. †Angles in parentheses measured to hydrogen of donor atom. Polyamide atoms labeled as shown (Fig. 2A).

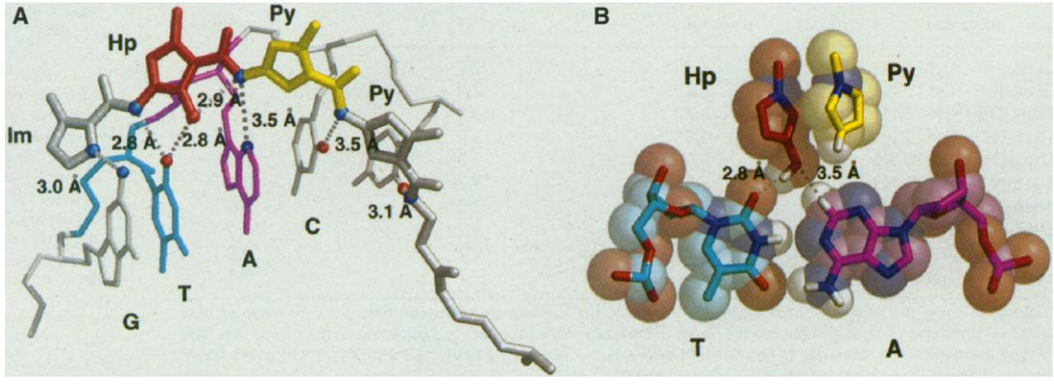

Fig. 3. (**A**) The hydrogen bonds between ImHpPyPy and one strand of DNA, indicated by dashed lines. (**B**) Space-filling model of the Hp/Py pair interacting with the T·A base pair shows that the Hp-OH tightly fits the cleft formed by the adenine-C2H. Figures were prepared by use of Molscript, Bobscript, and Raster3D (*21*).

from ideal B-form by a strong propeller twist and opening of the target T·A base pairs. However, the Hp/Py pairs induce a change in the T·A base pairs from no shear (−0.2 average displacement between the bases in the base pair, perpendicular to the helix axis) to a large positive shear (1.2 Å, average) (Table 3). The movement of the bases past one another may result from the Hp-O6 contact with the adenine-C2, pressing the adenine of the target base pair back into the major groove. The increased displacement between the bases stretches the Watson-Crick hydrogen bonds between them by 0.5 Å, on average (Table 3, center portion). Although the specificity of Hp-containing polyamides is greatly increased for T·A compared with A·T, the affinities are slightly reduced relative to the Py counterparts. For example, ImHpPyPy-β-Dp and ImPyPyPy-β-Dp bind a 5′-AGTACT-3′ site with equilibrium dissociation constants of 344 and 48 nM, respectively (*17*). The energetic penalty due to the partial "melting" of the target T·A base pairs could account for the 1.2-kcal/mol reduction in binding affinity (*18*).

The change in the shear in the presence of the Hp/Py versus the Py/Py pair is more dramatic for one of the two crystallographically independent T·A base pairs than for the other (2.2 Å compared with 0.4 Å). A buffer molecule from the crystallization solution, tris-(hydroxymethyl)-aminomethane molecule (Tris), is bound in the major groove of this A·T base pair of the ImHpPyPy structure. No evidence for a corresponding buffer molecule was found in the major groove of the ImPyPyPy structure. The Tris molecule bound in the major groove selectively in the presence of an Hp/Py pair in the minor groove, suggesting that Hp-containing polyamides may be used as an indirect lever to manipulate interactions of proteins with the major groove.

The hydrogen bonds between the amides of each ImPyPyPy polyamide and the purine-N3 or pyrimidine-O2 of the adjacent DNA strand are maintained for the ImHpPyPy polyamide. However, the hydrogen bonds between the DNA and the ImHpPyPy amides are longer for the residues that follow the Hp than those observed for the ImPyPyPy complex (Table 2). The hydroxyl forms an intramolecular hydrogen bond with the following amide, causing the hydrogen bond of that amide with the adenine-N3 to become bifurcated and therefore weaker. This may be an additional source of the slightly decreased affinity of the Hp-containing polyamides relative to the Py counterparts.

These studies have established how a designed ligand can predictably discriminate A·T from T·A in the minor groove, using the double hydrogen bond acceptor potential of the thymine-O2 and the asymmetry of the adenine-C2 cleft (*8, 15*). The structure eliminates the possibilities that a bulky substitution at the Py 3-position might sterically clash with the thymine-O2 (*12*) or cause a gross distortion of the DNA duplex (*19*). In addition, the structural basis of minor groove recognition by a synthetic molecule raises the question of whether naturally occurring DNA binding proteins may use similar principles to distinguish between the base pairs in the minor groove (*20*).

Table 3. DNA conformation.

*Helical parameters**

Base pair	Shear† (Å)		Propeller twist‡ (°)		Opening§ (°)	
	ImHpPyPy	ImPyPyPy	ImHpPyPy	ImPyPyPy	ImHpPyPy	ImPyPyPy
5′ 3′						
G·C	−0.7	−0.7	−13.8	−8.8	3.6	−3.1
T·A	0.1	−0.3	−19.5	−24.5	−8.8	−14.3
A·T‖	2.2	0.0	−19.1	−27.5	−24.9	−27.5
C·G	−0.1	−0.1	−13.6	−5.8	−5.3	−5.8
3′ 5′						
B-DNA¶	0		4.1		−4.0	

Feature	ImHpPyPy	ImPyPyPy	B-DNA
Minor groove width (Å)	7.9	7.9	6.0
Sugar pucker (°)	C2′-endo	C2′-endo	C2′-endo
Helical twist (°)	35	35	36
Helical pitch (Å)	3.4	3.3	3.4

Watson-Crick hydrogen bond lengths for central GTAC

Base pair	ImHpPyPy (Å)	ImPyPyPy (Å)	Difference (Å)
Gua4-N2···Cyt17-O2	2.7	2.7	0.0
Gua4-N1···Cyt17-N3	2.8	2.9	0.1
Gua4-O6···Cyt17-N4	2.7	3.0	0.3
Thy5-N3···Ade16-N1	3.5	3.2	0.3
Thy5-O4···Ade16-N6	3.6	3.0	0.6
Ade6-N1···Thy15-N3	3.3	2.7	0.6
Ade6-N6···Thy15-O4	3.2	2.6	0.6
Cyt7-O2···Gua14-N2	2.6	2.7	0.1
Cyt7-N3···Gua14-N1	2.9	2.7	0.2
Cyt7-N4···Gua14-O6	3.0	2.7	0.3

*Calculated using the program Curves4 (*28*). †Shear is the displacement between base pairs, in plane of base pairs. ‡Propeller twist, angle between the planes of the bases in the base pair. §Opening, angle between the base pairs, in the plane of the bases, due to flexing about helix axis. ‖The base pair of the ImHpPyPy structure with bound Tris. ¶Ideal B-DNA generated using the program Insight.

References and Notes

1. N. C. Seeman, J. M. Rosenberg, A. Rich, *Proc. Natl. Acad. Sci. U.S.A.* **73**, 804 (1976).
2. T. A. Steitz, *Q. Rev. Biophys.* **23**, 203 (1990).
3. C. Branden and J. Tooze, *Introduction to Protein Structure* (Garland, New York, 1991), p. 83.
4. Y. Choo and A. Klug, *Curr. Opin. Struct. Biol.* **7**, 117 (1997).
5. W. S. Wade, M. M. Mrksich, P. B. Dervan, *J. Am. Chem. Soc.* **114**, 8783 (1992); J. W. Trauger, E. E. Baird, P. B. Dervan, *Nature* **382**, 559 (1996); S. White, E. E. Baird, P. B. Dervan, *Chem. Biol.* **4**, 569 (1997).
6. J. M. Gottesfeld, L. Neely, J. W. Trauger, E. E. Baird, P. B. Dervan, *Nature* **387**, 202 (1997).
7. M. Mrksich *et al.*, *Proc. Natl. Acad. Sci. U.S.A.* **89**, 7586 (1992); B. H. Geierstanger, M. Mrksich, P. B. Dervan, D. E. Wemmer, *Science* **266**, 646 (1994); C. L. Kielkopf, E. E. Baird, P. B. Dervan, D. C. Rees, *Nature Struct. Biol.* **5**, 104 (1998).
8. S. White, J. W. Szewczyk, J. M. Turner, E. E. Baird, P. B. Dervan, *Nature* **391**, 468 (1998).
9. S. White, E. E. Baird, P. B. Dervan, *Biochemistry* **35**, 6147 (1996).
10. J. G. Pelton and D. E. Wemmer, *Proc. Natl. Acad. Sci. U.S.A.* **86**, 7586 (1989).
11. S. White, E. E. Baird, P. B. Dervan, *J. Am. Chem. Soc.* **119**, 6953 (1997).
12. M. L. Kopka *et al.*, *Structure* **5**, 1033 (1997).
13. X. Chen, B. Ramakrishnana, S. T. Rao, M. Sundaralingam, *Nature Struct. Biol.* **1**, 169 (1994).
14. E. N. Baker and R. E. Hubbard, *Prog. Biophys. Mol. Biol.* **44**, 97 (1984).
15. J. M. Wong and E. Bateman, *Nucleic Acids Res.* **22**, 1890 (1994).
16. M. C. Wahl and M. S. Sundaralingam, *Trends Biochem. Sci.* **22**, 98 (1997).
17. Equilibrium dissociation constants were determined by quantitative DNase I footprint titration experiments on the DNA restriction fragment pJT8 (*6*) as described (*11*).
18. K. Brameld, S. Dasgupta, W. A. Goddard, *J. Am. Phys. Chem. B* **101**, 4851 (1997).
19. Y. Kim, J. H. Geiger, S. Hahn, P. B. Sigler, *Nature* **365**, 512 (1993); J. L. Kim, D. B. Nikolov, S. K. Burley, *ibid.*, p. 520.
20. For example, certain high-mobility group–domain proteins recognize a TT step with a conserved tyrosine that has been suggested to hydrogen bond with the thymine-O2 and pack against the adenine-C2 [A. A. Travers, *Nature Struct. Biol.* **2**, 615 (1995)], and the NH_2-terminal arm of homeodomain proteins has weak T·A specificity [S. E. Ades and R. T. Sauer, *Biochemistry* **34**, 14601 (1995)], which may or may not be related to an arginine side chain that satisfies two hydrogen bonds with the thymine-O2 [D. S. Wilson, B. Guether, C. Desplan, J. Kuriyan, *Cell* **82**, 709 (1995); J. A. Hirsch and A. K. Aggarwal, *EMBO J.* **14**, 6280 (1995); L. Tucker-Kellogg *et al.*, *Structure* **5**, 1047 (1997)].
21. D. J. Bacon and W. F. A. Anderson, *J. Mol. Graph.* **6**, 219 (1988); P. J. Kraulis, *J. Appl. Crystallogr.* **24**, 946

(1991); K. A. Nicholls, R. Baradwaj, B. Honig, *Biophys. J.* **64**, a166 (1993); E. A. Merrit and M. E. Murphy, *Acta Crystallogr. D* **50**, 869 (1994); R. Esnouf, *J. Mol. Graph.* **15**, 133 (1997).

22. We synthesized the polyamides ImHpPyPy-β-Dp and ImPyPyPy-β-Dp by solid-phase methods [E. E. Baird and P. B. Dervan, *J. Am. Chem. Soc.* **118**, 6141 (1996)] using Boc-protected 3-methoxypyrrole, imidazole, and pyrrole amino acids. Identity and purity of the polyamides was confirmed by ^{1}H nuclear magnetic resonance and matrix-assisted laser-desorption ionization time-of-flight mass spectrometry. Synthetic deoxyoligonucleotides were synthesized without removal of the 5′-dimethoxy-trityl group and purified with two rounds of reversed-phase fast-protein liquid chromatography on a C8 column (Pharmacia). The ImHpPyPy and ImPyPyPy·5′-CC**AG-TACT**GG-3′ crystals grew under similar conditions to those of ImImPyPy·5′-CC**AGGCCT**GG-3′.
23. J. Navaza, *Acta Crystallogr. A* **50**, 157 (1994).
24. Z. Otwinowski, in *Data Collection and Processing*, N. I. L. Sawyer and S. Bailey, Ed. (SERC Daresbury Laboratory, UK, 1993), pp. 56–61.
25. T. A. Brunger, *X-PLOR Version 3.1: A System for X-ray Crystallography and NMR* (Yale Univ. Press, New Haven, CT, 1992).
26. G. J. Kleygwegt and T. A. Jones, in *From First Map to Final Model*, R. Hubbard and D. A. Waller, Ed. (SERC Daresbury Laboratory, UK, 1994), pp. 59–66.
27. G. Parkinson, J. Vojtechovsky, L. Clowney, A. T. Brunger, H. M. Berman, *Acta Crystallogr. A* **47**, 110 (1991).
28. R. Lavery and H. Sklenar, *J. Biomol. Struct. Dyn.* **6**, 63 (1988).

29. We are grateful to the NIH for research support, to the NSF for a predoctoral fellowship to C.L.K., to J. Edward Richter for an undergraduate fellowship to J.M.T., and to the Howard Hughes Medical Institute for a predoctoral fellowship to E.E.B. We thank J. E. Wedekind, C. L. Drennan, T. M. Iverson, and M. Williamson for assistance with data collection and S. Horvath for oligonucleotide synthesis. The rotation camera facility at SSRL is supported by the U.S. Department of Energy and NIH. Coordinates have been deposited in the Nucleic Acid Database with accession numbers BDD002 (ImHpPyPy) and BDD003 (ImPyPyPy).

26 June 1998; accepted 25 August 1998

A Carrot Leucine-Rich–Repeat Protein That Inhibits Ice Recrystallization

Dawn Worrall, Luisa Elias, David Ashford, Maggie Smallwood,* Chris Sidebottom, Peter Lillford, Julia Telford, Chris Holt, Dianna Bowles

Many organisms adapted to live at subzero temperatures express antifreeze proteins that improve their tolerance to freezing. Although structurally diverse, all antifreeze proteins interact with ice surfaces, depress the freezing temperature of aqueous solutions, and inhibit ice crystal growth. A protein purified from carrot shares these functional features with antifreeze proteins of fish. Expression of the carrot complementary DNA in tobacco resulted in the accumulation of antifreeze activity in the apoplast of plants grown at greenhouse temperatures. The sequence of carrot antifreeze protein is similar to that of polygalacturonase inhibitor proteins and contains leucine-rich repeats.

Living organisms have developed diverse strategies to enable them to survive freezing conditions. One strategy that has evolved repeatedly is the expression of antifreeze proteins (AFPs) (*1*, *2*). AFPs cause thermal hysteresis (TH) and inhibit ice recrystallization. TH, in which the freezing temperature is lower than the melting temperature, allows freeze-avoiding organisms such as fish to supercool in the presence of ice. Ice recrystallization, the growth of large ice crystals at the expense of smaller ones, is one cause of tissue damage in freeze-tolerant organisms. Both TH and recrystallization inhibition (RI) activity are thought to result from interaction of AFPs with ice crystal surfaces (*2*, *3*).

TH activity has been detected in at least 26 species of higher plants (*4*), and some candidate proteins have been purified (*5*–*7*). However, the TH values exhibited by these extracts are low (0.2° to 0.6°C) in the context of the environmental temperatures that plants encounter. Plant AFPs are therefore unlikely to function to lower the temperature at which ice crystallizes in the apoplast but rather to inhibit the potentially damaging process of ice recrystallization. Here, we describe purification of an active AFP from cold-acclimated carrot tap roots and the cloning and expression of the corresponding cDNA.

D. Worrall, L. Elias, D. Ashford, M. Smallwood, D. Bowles, The Plant Laboratory, Biology Department, University of York, Post Office Box 373, York, YO1 5YW, UK. C. Sidebottom, P. Lillford, J. Telford, C. Holt, Unilever Research, Colworth House, Sharnbrook, Bedford, MK44 1LO, UK.

*To whom correspondence should be addressed.

Using biochemical separation techniques (*8*), we isolated a 36-kD glycoprotein from cold-acclimated carrot tap root that copurified with RI activity (Fig. 1). The purified AFP was assayed for TH, and a value of 0.35°C was detected (*9*).

The carrot AFP was found to be N-glycosylated (Fig. 2) (*10*); however, enzymic removal of the small glycan side chain did not affect its RI activity. This result contrasts with the *Solanum* active or the fish antifreeze glycor protein (AFGP), which lost activity on removal of their glycan groups (*6*, *11*).

The amino acid sequence of internal peptides was obtained (*12*), and the coding region corresponding to the purified protein was isolated from a cold-acclimated carrot root cDNA library (*13*) (Fig. 3A). The predicted features of the deduced AFP sequence correlate well with those determined empirically for the purified carrot protein. The apparent relative molecular mass (M_r) of the native protein on SDS–polyacrylamide gel electrophoresis (PAGE) was 36 kD, and its isoelectric point was 5.0, compared with 34 kD and 4.8 for the deduced protein. The deduced protein had three potential N-glycosylation sites, at least one of which appears to be occupied in the native protein, and a putative signal peptide.

The AFP cDNA was fused to a double cauliflower mosaic virus *35S* promoter, and

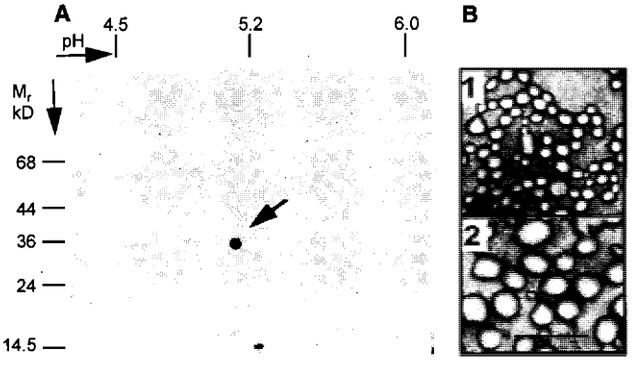

Fig. 1. RI activity of purified carrot AFP. (**A**) Two-dimensional PAGE separation of purified carrot AFP. Carrot antifreeze activity, purified as described previously (*8*), was separated by isoelectric focusing– and SDS-PAGE (*27*), and the gel was stained with Coomassie blue. (**B**) The same material was adjusted to a protein concentration of 1.5 μg/ml and assayed for RI (*8*). Ice crystals remained small in the sample containing purified carrot AFP (panel 1) compared with ice crystals in a control sample (panel 2). Scale bar, 100 μm.